Chinese Chemical Letters 31 (2020) 2789–2794

Contents lists available at ScienceDirect

Chinese Chemical Letters

journal homepage: www.elsevier.com/locate/cclet

Communication

Bifunctional copper modified graphitic carbon nitride catalysts for efficient tetracycline removal: Synergy of adsorption and photocatalytic degradation

Huijing Wang[a], Jun Zhang[a,*], Pu Wang[a], Linlin Yin[a], Yu Tian[a], Junjing Li[b]

[a] State Key Laboratory of Urban Water Resources and Environment (SKLUWRE), School of Environment, Harbin Institute of Technology, Harbin 150090, China
[b] State Key Laboratory of Separation Membranes and Membrane Processes, School of Environmental and Chemical Engineering, Tianjin Polytechnic University, Tianjin 300387, China

ARTICLE INFO

Article history:
Received 13 March 2020
Received in revised form 3 July 2020
Accepted 17 July 2020
Available online 30 July 2020

Keywords:
Carbon nitride
Tetracycline
Adsorption
Photocatalysis
Environment remediation

ABSTRACT

In order to efficiently remove tetracycline in wastewater through the synergistic effect of adsorption and photocatalytic degradation, a series of novel composite materials (Cu doped g-C_3N_4) were synthesized by two-pot hydrothermal method. It was found that the composite materials with optimized ratio (Cu/CN-1) displayed outstanding adsorption and photocatalytic performance as compared with pure g-C_3N_4 photocatalyst. The removal efficiency of tetracycline (TC, 50 mg/L) reached almost 99% within 30 min by Cu/CN-1 through the synergy of adsorption and photocatalysis under visible-light irradiation, which was the highest removal efficiency ever reported. The adsorption kinetics and isotherms of TC on the Cu/CN-1 were well fitted with the *pseudo*-second-order kinetic model and Langmuir model, respectively. Moreover, it was confirmed that the main effective reactive groups were $O_2^{\bullet-}$ and h^+ in photocatalytic process. The Cu/CN-1 exhibited high stability and excellent reusability after five cycle experiments. Finally, the mechanism of synergy between Cu and g-C_3N_4 was proposed: on the one hand, the decoration of Cu particles significantly increased the adsorption sites of Cu/CN-1 to tetracycline, on the other hand, the modification of Cu particles effectively inhibits charge recombination and broadens the visible light absorption range of the photocatalyst.This study provided a promising photocatalyst to be used for TC removal in the actual wastewater.

Significant concerns have been raised over the residues of pharmaceutical antibiotics in water matrix. Among all of the antibiotics, tetracycline (TC) as one of the most commonly used antibiotics is proverbially applied in disease therapy and livestock feed due to its excellent ability to conquer many different kinds of pathogenic bacteria [1–4]. However, only a small section of TC can be assimilated by the human or animals and the remaining is indirectly discharged into environmental matrix through metabolism, and these residues can be enriched and concentrated through food chain arousing potential threats on ecosystems and human health [5,6]. Therefore, it is imperative to remove tetracycline from the water matrix for the ecological environment and human health [7,8].

The conventional treatment technology including physical adsorption and biological degradation have been employed to deal with tetracycline from aqueous solution. However, physical adsorption suffers low purification efficiency, regeneration difficulties and non-degradable properties, and biological degradation could not long-term effectively remove tetracycline in wastewater due to its bacterial resistance. Therefore, developing more efficient, economical and environmentally friendly processes for the removal of tetracycline in water matrix still remains a challenge. As promising methods, the advanced oxidation processes (AOPs) have exhibited the predominance in removing the recalcitrant and unbiodegradable tetracycline, and it works mainly by the generation of highly oxidizing hydroxyl radicals to efficiently oxidize series of organic compounds. So far, different kinds of advanced oxidation processes have been employed to degrade tetracycline including Fenton reagent oxidation [9], ozonation [10], electrochemical oxidation [11] and photocatalytic oxidation [12] processes. Among them, the photocatalytic technique is considered more desirable for the degradation of tetracyclines owing to its economical, efficient, and environmentally friendly advantages compared with other advanced oxidation processes.

Semiconductor catalysts design is widely explored as the main part of photocatalytic oxidation technology. In recent years, the graphitic carbon nitride (g-C_3N_4) has attracted much attention of

* Corresponding author.
E-mail address: hitsunyboy@126.com (J. Zhang).

https://doi.org/10.1016/j.cclet.2020.07.043
1001-8417/

researchers because of its high stability, non-toxicity, good accessibility and adjustable band gap energy [13–16]. Currently, the g-C_3N_4 has already played an important part in many fields such as environmental restoration, waste water purification and synthetic organic chemistry [17–20]. However, it also exists some inadequacies, for example, the removal efficiency is not completely satisfactory for the refractory antibiotics in water matrix, specifically tetracycline [21,22]. The photocatalyst achieves degradation of tetracycline into small molecular by generating active oxygen species with strong oxidative properties, but the active oxygen species are easy to quench when migrating from photocatalyst surface into solution, which property of active oxygen species limits the active site of the redox reaction to the catalyst surface. To compensate for these shortcomings, various strategies have been used, such as constructing various topographical structures [23,24], doping metal elements [25], and coupling with other materials to form heterojunctions [26–28].

Our previous study found that copper particles have excellent adsorption properties for tetracycline. Considering introducing copper particles into carbon nitride, the issue of poor adsorption performance of carbon nitride for tetracycline may be resolved. The increased adsorption sites on the surface of carbon nitride may enhance the photocatalytic effect of carbon nitride on tetracycline. In this work, novel Cu particles doped graphitic carbon nitride composite materials were synthesized by a facile hydrothermal method. The adsorption and visible-light-driven photocatalytic properties of the as-synthesized composite materials towards TC were systematically investigated. The feasible mechanism of Cu on the adsorption and photocatalytic performance of g-C_3N_4 was discussed based on the related characterizations and experiment analysis.

To analyze the crystal structure of the as-synthesized samples, the X-ray diffraction (XRD) diffraction pattern of bare Cu, pure g-C_3N4 and modified Cu/CN-X were shown in Fig. 1a. The XRD peaks at $2\theta = 27.2^\circ$ and 12.7° were indexed as the (002) plane and the (110) plane, respectively, corresponding to the diffraction peaks caused by the s-triazine ring and conjugated aromatic systems in g-C_3N_4 with graphitic structure (JCPDS No. 87-1526). In Fig. 1a, according to the JCPDS card No. 45-0937, the peak at 36.2° corresponds to the (111) plane of CuO. As shown diffraction peaks in pristine Cu and Cu/CN-X samples, the peaks located at $2\theta = 43.3^\circ$, 50.43° and 73.13° corresponded to (111), (200), (220) diffraction crystal planes of Cu according to JCPDS card No. 04-0836, respectively. Compared with the pristine g-C_3N_4 and Cu samples, the composite samples Cu/CN-0.5 and Cu/CN-1 included all diffraction peaks of both g-C_3N_4 and Cu but with a broader and lower peak intensity than them, which may be owing to more defects in the structure of the composite samples, as compared with the pure samples. The 27.2° peaks of composite samples shifted gradually towards the higher angle with increasing Cu particles content. This indicated that the decrease in the gallery distance between the interplanar g-C_3N_4 layers was attributed to the distortion in the in-plane aromatic stacking by Cu particles dopant, proving that the Cu/CN-X composite samples were synthesized successfully [29,30].

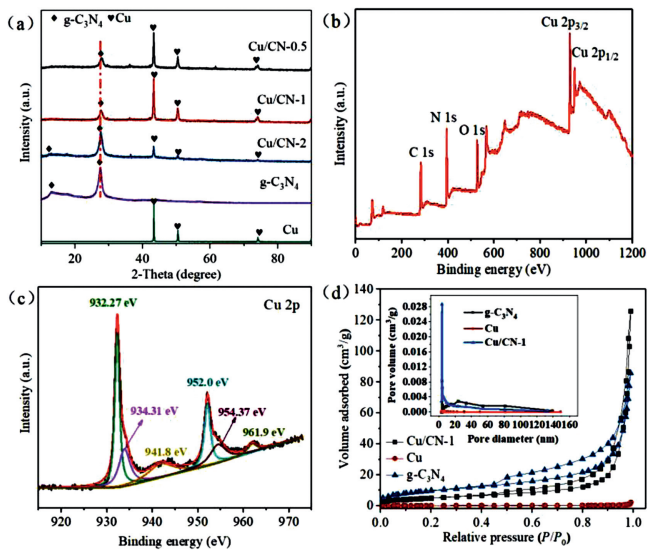

Fig. 1. (a) XRD patterns of Cu, g-C_3N_4 and different composites of Cu/CN-0.5, Cu/CN-1, Cu/CN-2. (b) and (c) The XPS spectra of Cu/CN-1. (d) Nitrogen adsorption-desorption isotherms and the corresponding pore size distributions curve (inset) of Cu, g-C_3N_4 and Cu/CN-1.

The X-ray photoelectron spectroscopy (XPS) was employed to characterize the valence and bonding of elements in Cu/CN-1 and the result was displayed in Figs. 1b and c. It was shown that all the four elements of C, N, O and Cu existed in the Cu/CN-1. The deconvolution peaks of Cu 2p was displayed in the Fig. 1c, the two predominant peaks focused on 932.27 eV and 952.08 eV were ascribed to the spin-orbit of Cu element in samples, and another two peaks located at 933.86 eV and 954.37 eV can be attributed to Cu^{2+} species attaching to the surface of Cu, causing by the oxidation of Cu element during hydrothermal reaction. The two satellite peaks situated at 944.5 eV and 963.2 eV can be attributed to the $2p_{3/2}$ and $2p_{1/2}$ ionization of outer electrons in Cu^{2+} [31]. Regularly, the Cu^+ and Cu possess nearly the same peak location both in $2p_{3/2}$ and $2p_{1/2}$, causing the difficulty in distinguishing the existence of Cu^+ or Cu. However, according to previous reports [32], the $2p_{3/2}$ binding energy discrepancy of CuO and Cu_2O was about 1.3 eV, and that of CuO and Cu was about 2.1 eV. The latter were obviously well matched our studies with 2.03 eV, confirming the presence of CuO. It was reported that a little amount of Cu^{2+} was beneficial to the stability of nanocomposite [33]. The high resolution spectrum of C 1s, O 1s and N 1s were showed in Fig. S1 (Supporting information), and the C 1s exhibits three peaks at 284.4 eV, 285.9 eV and 287.4 eV corresponding to the sp^2 of graphite carbon atom C–C, C–O, and N-C=N in the sp^2-hybridized carbon of the aromatic ring of g-C_3N_4, respectively. The O 1s were divided into two peaks corresponding to the lattice oxygen in CuO and oxygen species adsorbed on the surface of the samples, and the N 1s spectra showed three main peaks at around 398.2, 399.9 and 405 eV corresponding to the C–N=C in the triazine rings, the tertiary nitrogen groups, and the uncondensed amino functions of g-C_3N_4, respectively.

The N_2 adsorption-desorption isotherms were executed in order to investigate the specific surface area and porosity of the prepared samples. As shown in Fig. 1d, both g-C_3N_4 and Cu/CN-1 exhibited analogous type IV N_2 adsorption -desorption isotherms with an H3 types of hysteresis loops, which manifested the mesoporous characteristics of the samples, specifically, explaining that the interconnected pore structure may be existed inside the samples. In particular, the specific surface area values of g-C_3N_4 and composite samples (Table S1 in Supporting information) were calculated indicating the composite samples was twice as much as g-C_3N_4 corresponding to 35.304 cm^2/g and 18.244 cm^2/g, respectively. Fig. 1d (the inset) showed the pore size distribution of the samples by employing the Barrett-Joyner-Halenda (BJH) method. It showed that g-C_3N_4 and composite samples have similar mesoporosity with 3.807 for g-C_3N_4 and 3.817 for composite samples. Other than that, it was also seen that g-C_3N_4 aperture curve existed a slight bulge at 23 nm and composite samples aperture curve possessed a continuously dropping distribution intensity from 3.827 nm to 32 nm, proving the existence of both micropores and mesopores in two samples, which was consistent with the curve jump at low specific pressure (about $P/P_0 = 0.45$) in Fig. 1d. However, the Cu almost had no hysteresis loop and the pore

size distribution curve was turned into a line, indicating the small surface area (0.402 cm^2/g) and disappearance of pores.

According to the scanning electron microscope (SEM) images of Cu and Cu/CN-1 in Figs. S2a and b (Supporting information), clearly, the size of Cu particle was about 0.8−1 μm with a polyhedron morphology of surface defects. Fig. S2b showed that Cu/CN-1 holds obvious layered morphology over the entire surface consisting of nanosheets with mass wrinkles. Furthermore, it was apparently found that Cu particles distribute in both the surface and the gully gap of g-C_3N_4. This appearance was excellent in consistent with TEM images of Cu/CN-1 in Fig. S2c (Supporting information). The SEM image of (a) Cu/CN-0.5 and (b) Cu/CN-2 were shown in Fig. S3 (Supporting information). Combined with the SEM image of Cu/CN-1 in Fig. S2b, it can be seen that as the mass ratio of Cu increases, the Cu load on the sample surface increases significantly. In Cu/CN-2, the g-C_3N_4 surface is almost entirely covered with Cu, which leads to a decrease in the photocatalytic activity of g-C_3N_4 because it can not be exposed to visible light. However, when the mass ratio of Cu is low, the Cu/CN-0.5 also does not have the best degradation ability due to the lack of adsorption-photocatalysis synergistic active sites.The HRTEM (Fig. S2d in Supporting information) was used to exhibit the morphological characteristics of Cu/CN-1. The characteristic fringes with an interplanar spacing of 0.223 nm, 0.258 nm and 0.312 nm were observed, which could be indexed as the (111) plane of Cu, (111) plane of CuO and (002) plane of g-C_3N_4, respectively. This was consistent with the XPS results as described above. As presented in the elemental mapping analysis of Cu/CN-1 (Fig. S2e in Supporting information), all atoms in the composite showed excellent dispersity, illustrating the Cu particles were evenly dispersed on the g-C_3N_4.

The TC adsorption capacity of as-synthesized samples were shown in Fig. S4a (Supporting information). It can be seen that the Cu/CN-1 composite sample exhibits more excellent adsorption ability accompanied with about 90% of TC (50 mg/L) removal within 120 min compared with only 80% of TC removal by Cu-CN-0.5 and about 76% by Cu/CN-2 during the same period. The adsorption efficiency of copper particle for TC was 55% at the same time, while g-C_3N_4 was only about 2%. The weak adsorption of g-C_3N_4 may be derived from the voids or flaws on the surface of the tri-*s*-triazine units [34]. The enhanced adsorption capacity of composite material may be attributed to both the increased specific surface area (Table S1) and excellent dispersion of Cu on the g-C_3N_4 (Fig. S2e).

The adsorption capacity of the Cu/CN-1 composite at different initial concentrations of TC solution was also studied shown in Fig. S4b (Supporting information). Further, to make a thorough inquiry in the rate-controlling step in the adsorption process, the *pseudo*-first-order, *pseudo*-second-order, and intraparticle diffusion models were exploited to fit the kinetics data in our studies, and the three kinds of kinetics models fitting curve were shown in Figs. S4c-e (Supporting information). The fitted kinetic parameters and the calculated correlation coefficients were given in Table S2 (Supporting information). The R^2 values of *pseudo*-second-order model ($0.9931 < R^2 < 0.9995$) at any concentrations researched were higher than that of *pseudo*-first-order model ($0.9019 < R^2 < 0.9521$), which indicated that the *pseudo*-second-order model was more precise for explicating the adsorption characteristics of TC onto Cu/CN-1. As reported, the *pseudo*-second-order kinetics model assumed mainly that the sorption rate is controlled by chemical sorption and the sorption capacity was proportional to the number of active sites on the adsorbent [35–37], which implied that the adsorption behaviour of TC by Cu/CN-1 mainly relied on chemical interactions. In order to further elucidate the diffusion mechanism and identify the steps involved in the adsorption process, the intra-particle diffusion model was employed. It clearly observed that the intra-particle diffusion was divided into three steps with different slopes, which indicated that multiple speed control factors arise during the adsorption process. The above three-part region with a gradually slower slope was attributed to the external surface diffusion adsorption, intraparticle diffusion adsorption, equilibrium intraparticle diffusion adsorption [38,39], respectively, which was the rate- controlled factors at each stage. Other than that, all extend lines without passing through the origin illustrated that the intraparticle diffusion was not sole rate-controlling step [40].

The Langmuir, Freundlich and Temkin isotherm were employed to evaluate the adsorption capacity of Cu/CN-1, as shown in Fig. S5 (Supporting information), and the isotherm fitting data were presented in Table S3 (Supporting information). In comparison with Freundlich isotherm, the Langmuir equation was more suitable for adsorption behaviour of TC on Cu/CN-1 ($R^2 = 0.9986$) compared with the Freundlich ($R^2 = 0.7608$) and Temkin ($R^2 = 0.9452$), which demonstrated a monolayer adsorption model of TC on Cu/CN-1. The Langmuir model was based on the assumption that adsorption was localized on a monolayer and all adsorption sites at the adsorbent were homogeneous [41,42].

The photocatalytic degraded capabilities of Cu/CN-0.5, Cu/CN-1, Cu/CN-2, Cu and g-C_3N_4 for TC solution under visible-light illumination were investigated and shown in Fig. 2, the blank experiment without any catalyst was used to evaluate the effect of illumination on the TC solution. It can be found that the TC solution without any catalyst hardly be photodegraded, while the Cu/CN-1 possessed the best photocatalytic performance among these samples with 99% of TC degradation rate within 30 min. The Cu/CN-0.5 and Cu/CN-2 had similar photocatalytic degradation effects showing 80% and 90% TC degradation within 60 min, respectively. It can be noticed that the removal rates of four samples for TC were all enhanced under visible-light illumination. Under the presence of free radicals, the possible degradation path of tetracycline was proposed. TC loses methyl group, $-CONH_2$ group loss, hydroxylation addition reaction, ring opening reaction in turn. Finally, TC can be completely mineralized into carbon dioxide and water [43,44].

The active free radical capturing experiments were conducted to reveal the main effective reactive groups in the process of photocatalytic degradation. Specifically, the radical scavengers of IPA, BQ, EDTA-2Na and $AgNO_3$ were engaged to capture $^{\bullet}OH$, $O_2^{\bullet-}$, h^+ and e^-, respectively. From Fig. S6a (Supporting information), the photocatalytic activity of the Cu/CN-1 was more remarkably suppressed in the presence of $AgNO_3$, EDTA-2Na and BQ compared those of IPA, which indicated that $O_2^{\bullet-}$ and h^+ played mainly part during photocatalytic degradation process.

The five cycles recycling experiments of Cu/CN-1 were carried out with the same operating condition to explore the reusable performance. According to Fig. S6b (Supporting information), the removal performance for TC has slight decrease during the second

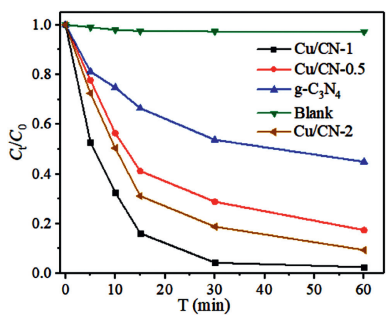

Fig. 2. Photocatalytic degradation of TC under the visible-light illumination by Cu/CN-1.

cycle experiment compared to the first experiment, but worthing noting that there was still holds 96% of TC removal. The TC removal efficiency remained around 92% even after four consecutive cycles, indicating that as-prepared Cu/CN-1 is a stable visible-light-driven photocatalyst.

The residual Cu concentration in the TC solution was detected under different pH values to evaluate the stability and non-polluting of the adsorbent. As shown in Table S4 (Supporting information), H^+ may be responsible for Cu ions leaching of Cu particles. It can be confirmed that the Cu/CN-1 composites were not suitable for application under excessive low and high pH. When pH ranged from 5.0–7.0, leaching concentration of Cu ion was in a low level and completely matched the EPA-US, and WHO Guidelines [45].

The adsorption is one of the effective physical processes for the removal of TCs from the wastewater [38]. It has been reported that the adsorption of TC on metal oxides is greatly affected by the pH of the solution [46]. As observed in Fig. S7 (Supporting information), The Cu/CN-1 adsorption capacity for TC at different pH values under adsorption equilibrium was demonstrated, which revealed under strong acid and alkaline conditions, the adsorption behaviour of the composite was significantly inhibited accompanied by low levels of adsorption capacity. However, the composite samples had a remarkably superior adsorption capacity when the solution was neutral and weakly acidic, and it was worth noting that in the range of pH 5–7, the adsorption rate of TC was up to 99% or more. According to foregoing reports, pH can affect the adsorption behaviour by altering the surface electrical of solid samples and the degree of ionization and form of ions of tetracycline in solution [47]. For example, tetracycline existed mostly as cation at strong acidic ambiance, as zwitterion at acidic conditions, and as an anion at alkaline environment. Furthermore, electrostatic repulsive force between composites with positive charge and tetracycline with cation contributed to the weak adsorption capacity at strong acidic conditions. It was also worth considering that the slight loss of copper particles deposited on g-C_3N_4 harried the composite structure in acidic conditions may be another reason. The Cu/CN-1 showed best adsorption capacity at pH from 5 to 7, and it was reasonable to exclude the lowest electrostatic repulsion effect of tetracycline with zwitterion on the adsorption process, which was consistent with the previous report [48]. At last, the competitive adsorption between the hydroxyl groups and tetracycline anion should be responsible for low adsorption capacity of sample. However, some specific interaction, such as surface complexation, could still be formed, probably between Cu ions and the amino groups [49,50].

The FTIR spectra of Cu/CN-1 before and after TC adsorption were shown in Fig. S8 (Supporting information). The band of 598 cm^{-1} was attributed to the Cu-O bond in Cu/CN-1. After adsorbing TC, the peak at 598 cm^{-1} moves to 599 cm^{-1}. The peak of Cu/CN-1 at 807 cm^{-1} can be assigned to the out-of-plane bending vibration of the s-triazine ring [51,52]. The FTIR spectra of Cu before and after TC adsorption were shown in Fig. S8 (Supporting information). The band of Cu adsorbent at 3430 cm^{-1} and 2920 cm^{-1} were attributed to the stretching vibration of O—H bond and C–H bond, respectively [53]. After adsorption, the peak of the hydrogen-oxygen bond shifted significantly located at 3410 cm^{-1}. The characteristic peaks at 1700–1200 cm^{-1} were mainly caused by the skeleton vibration of the benzene ring in the tetracycline molecule [54]. The appearance of peaks at 1445 cm^{-1} after adsorbing was assigned to the skeleton vibration of the benzene ring in tetracycline, and the band of Cu-O bond at 597 cm^{-1} shifted to 599 cm^{-1} after tetracycline adsorption and the characteristic peaks at 1700–1200 cm^{-1} became sharper. All those changes demonstrated that the tetracycline molecule was successfully adsorbed on the Cu, and the adsorption process may cause by the formation of hydrogen bonding and cation-π interaction between copper particles and tetracycline molecules.

The UV–vis diffuse reflectance spectroscopy was used to probe the optical activities and probable photo-catalytic efficiencies of as-synthesized samples. As depicted in Fig. 3a, it could be seen that the composite samples had a stronger light absorption than bare g-C_3N_4 especially in the 450–700 nm wavelength region. The widened absorption peak can be ascribed to d-d transitions of Cu^{2+} ions which were embedded in the framework of g-C_3N_4 [55]. The calculated band gap energies (E_g) was also shown in Fig. 3a (inset), the band gap of bare g-C_3N_4 (E_g =2.23 eV) was lower than that of composite samples (E_g =2.80 eV), which indicated that by incorporating the Cu into the g-C_3N_4, more electron-hole pairs could be generated under visible light irradiation, and promoted the photocatalytic activity.

The PL spectra was employed to explore the recombination efficiency of photogenerated electron-hole pairs of three samples, and the results were displayed in Fig. 3b. It could be found that compared to the Cu and g-C_3N_4, the Cu/CN-1 composite showed a lower peak intensity, indicating that the Cu/CN-1 composite owned a lower photogenerated electron-hole recombination efficiency, which meant higher photocatalytic degradation ability. Simultaneously, the electrochemical impedance spectra (EIS) (Fig. 3c) suggested that the Cu/CN-1 composite exhibited a smaller arc diameter than g-C_3N_4, and in general, a smaller diameter of the semi-circular curve represented a smaller charge transfer resistance [56]. The Cu particles showed in the inset of Fig. 3c owned the smallest arc diameter due to its excellent metal conductivity. As analysed above, the Cu particles existing in composite could inhibit the photogenerated electron-hole pairs recombination by transferring the electron from g-C_3N_4 to Cu particle, which could profoundly facilitate the photocatalytic activities of Cu/CN-1. To further confirm the fact of the separation and transfer of photogenerated electron-hole pairs, the photoelectric current curve of Cu/CN-1 and g-C_3N_4 were recorded. As displayed in the Fig. 3d, it was obviously observed that the Cu/CN-1 exhibited a higher transient photocurrent intensity than g-C_3N_4 indicating more separation of photogenerated electron-hole pairs in Cu/CN-1. Other than this, the reversible and stable transient photocurrent responses curves of Cu/CN-1 and g-C_3N_4 suggested the good

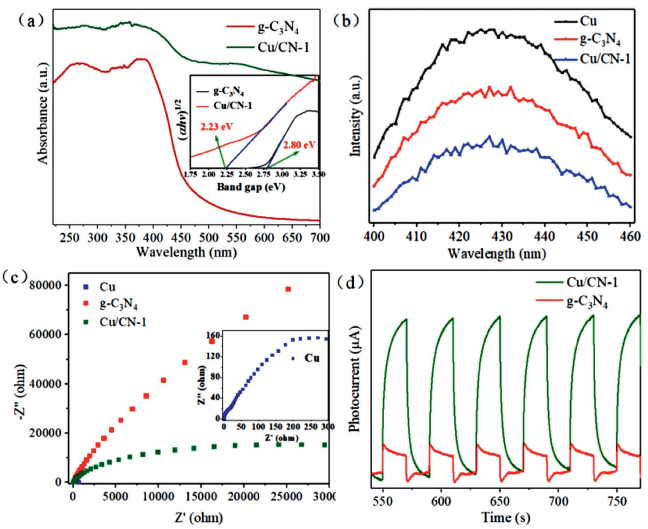

Fig. 3. (a) UV–vis diffuse reflectance of g-C_3N_4 and Cu/CN-1 and plots of $(\alpha h\nu)^2$ *versus* photon energy ($h\nu$) of g-C_3N_4 and Cu/CN-1. (b) The Photoluminescence (PL) emission spectra, (c) electrochemical impedance spectra of Cu, g-C_3N_4 and Cu/CN-1 and (d) transient photocurrent response of g-C_3N_4, Cu/CN-1.

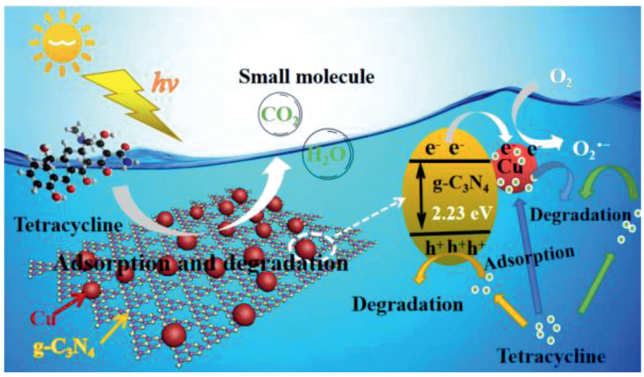

Scheme 1. Schematic diagram for the adsorption and photocatalytic mechanism of Cu/CN-1.

chemical structure stability and sensitive photoelectronic activities of samples [57].

The possible mechanism of improving the adsorption and photocatalytic efficient of as-synthesized samples was proposed (Scheme 1). Above all, the tetracycline was adsorbed on Cu particle surface through electrostatic attraction, hydrogen bonding and cation-π interaction, then electrons (e^-) in the valence band (VB) of g-C_3N_4 was excited and transferred to the CB of Cu under visible light irradiation, and further distracted to the Cu particle, the h^+ generated on the valance band (VB) of g-C_3N_4 was remained in the VB of g-C_3N_4, thus the e^- and h^+ was accumulated in Cu particle and the VB of g-C_3N_4, respectively, inhibiting the combination of photogenerated hole-electron pairs. Then the O_2 molecular obtained the electron existing in the Cu surface generating powerful reactive oxygen species $O_2^{\bullet-}$ which could quickily and effectively decompose the tetracycline adsorbed on Cu species macromolecule into small molecules. Meanwhile, the h^+ collected in the VB of g-C_3N_4 could oxidize tetracycline directly into small molecules, in which the increasing specific surface area improved adsorption and photocatalytic performance of Cu/CN-1.

Cu doped g-C_3N_4 composite material with different mass ratio were successfully synthesized through a two-pot hydrothermal method. Different from the precious metals, Cu exhibits excellent specific adsorption performance for TC, which means that Cu supported on g-C_3N_4 can further optimize the removal ability of TC based on the previous similar type composite materials. The proposed Cu/CN-1 photocatalyst showed a highly visible light photocatalytic degradation capability of TC, due to the decoration of Cu particles which could significantly increase the adsorption ability of Cu/CN-1 to TC. The enhanced adsorption capability was mainly ascribed to the electrostatic interaction, hydrogen bonding and surface complexation between Cu ions and the amino groups. Meanwhile, the modification of Cu species effectively enhanced visible-light photocatalytic degradation capability through improving visible-light absorption and suppressing the recombination of photogenerated electron-hole pairs. $O_2^{\bullet-}$ and h^+ as the dominant reactive species participate in the photocatalytic degradation of tetracycline. Furthermore, the removal efficiency of Cu/CN-1 composite had no significant reduction after five cycles of recycling. This study not only provides a novel material for efficient tetracycline removal but a meaningful strategy for the design of catalysts with both efficient of adsorption and photocatalytic degradation activity for tetracycline removal, which is greatly significant for the construction of high-efficiency photocatalysts.

Declaration of competing interest

The authors declare that they have no known competing financial interests or personal relationships that could have appeared to influence the work reported in this paper.

Acknowledgments

This study was supported by the National Key R&D Program of China (No. 2019YFD1100300), National Natural Science Foundation of China (Nos. 41877396, 51708157), Shenzhen Key Technology R&D Program of China (No. JSGG2018050718 3210868). The authors also appreciate the State Key Laboratory of Urban Water Resource and Environment, Harbin Institute of Technology (Nos. ES201905, 2020TS02) and State Key Laboratory of Separation Membranes and Membrane Processes (Tianjin Polytechnic University, No. M2-201701).

Appendix A. Supplementary data

Supplementary material related to this article can be found, in the online version, at doi:https://doi.org/10.1016/j.cclet.2020.07.043.

References

[1] K.J. Choi, S.G. Kim, C.W. Kim, S.H. Kim, Chemosphere 66 (2007) 977–984.
[2] Y. Wang, H. Zhang, J. Zhang, et al., J. Hazard. Mater. 192 (2011) 35–43.
[3] R. Daghrir, P. Drogui, Environ. Chem. Lett. 11 (2013) 209–227.
[4] D. Jiang, T. Wang, Q. Xu, et al., Appl. Catal. B: Environ. 201 (2017) 617–628.
[5] Z. Li, L. Zhu, W. Wu, S. Wang, L. Qiang, Appl. Catal. B: Environ. 192 (2016) 277–285.
[6] H. Xiong, D. Zou, D. Zhou, et al., Chem. Eng. J. 316 (2017) 7–14.
[7] R. Gothwal, T. Shashidhar, Air Water 43 (2015) 479–489.
[8] S. Gartiser, E. Urich, R. Alexy, K. Kummerer, Chemosphere 67 (2007) 604–613.
[9] A.G. Trovo, R.F. Nogueira, A. Aguera, et al., Water Res. 45 (2011) 1394–1402.
[10] Y. Yue, Z. Peng, W. Wang, et al., Powder Technol. 347 (2019) 211–219.
[11] Y. Wu, J. Lu, M. Meng, et al., Chem. Eng. J. 309 (2017) 263–271.
[12] C. Song, B.B. Guo, X.F. Sun, et al., Chem. Eng. J. 358 (2019) 1139–1146.
[13] F. Chen, Q. Yang, S. Wang, et al., Appl. Catal. B: Environ. 209 (2017) 493–505.
[14] Q. Gu, Y. Liao, L. Yin, et al., Appl. Catal. B: Environ. 165 (2015) 503–510.
[15] Y. Song, J. Qi, J. Tian, S. Gao, F. Cui, Chem. Eng. J. 341 (2018) 547–555.
[16] M. Wu, H. Lv, T. Wang, T. An, S. Wang, Catal. Today 315 (2018) 205–212.
[17] J. Chen, X. Xiao, Y. Wang, Z. Ye, Appl. Surf. Sci. 467 (2019) 1000–1010.
[18] L. Li, Z. Cai, Q. Wu, et al., J. Am. Chem. Soc. 138 (2016) 7681–7686.
[19] J. Xu, M. Fujitsuka, S. Kim, Z. Wang, T. Majima, et al., Appl. Catal. B: Environ. 241 (2019) 141–148.
[20] J. Xu, Z. Wang, Y. Zhu, ACS Appl. Mater. Interfaces 9 (2017) 27727–27735.
[21] H. Wang, Y. Wu, M. Feng, J.W. Chew, et al., Water Res. 144 (2018) 215–225.
[22] H. Yi, M. Yan, D. Huang, et al., Appl. Catal. B: Environ. 250 (2019) 52–62.
[23] S.C. Wang, Z.Y. Teng, Y.Q. Xu, et al., Appl. Catal. B: Environ. 260 (2020) 118145.
[24] Y. Luo, X. Wei, B. Gao, et al., Chem. Eng. J. 375 (2019) 122019.
[25] A. Shahzeydi, M. Ghiaci, H. Farrokhpour, et al., Chem. Eng. J. 370 (2019) 1310–1321.
[26] Y. Sheng, Z. Wei, H. Miao, et al., Chem. Eng. J. 370 (2019) 287–294.
[27] N. Li, Y. Tian, J. Zhao, et al., Chem. Eng. J. 352 (2018) 412–422.
[28] H. Sudrajat, J. Alloys. Compd. 716 (2017) 119–127.
[29] M. Zhou, M. Tian, C. Li, Chem 27 (2016) 1188–1199.
[30] M. Zhu, L.S. Zhang, S. Liu, et al., Chin. Chem. Lett. 31 (2020) 1961–1965.
[31] H. Zhang, Q.Q. Ji, L.D. Lai, G. Yao, B. Lai, Chin. Chem. Lett. 30 (2019) 1129–1132.
[32] C.K. Wu, M. Yin, S. O'Brien, J.T. Koberstein, Chem. Mater. 18 (2006) 6054–6058.
[33] J. Kang, H.J. Liu, Y.M. Zheng, J.H. Qu, J.P. Chen, J. Colloid Interface Sci. 344 (2010) 117–125.
[34] F.C. Wu, R.L. Tseng, R.S. Juang, J. Colloid Interf. Sci. 283 (2005) 49–56.
[35] W.R. Chen, C.H. Huang, Chemosphere 79 (2010) 779–785.
[36] L.L. Ji, W. Chen, L. Duan, D.Q. Zhu, Environ. Sci. Technol. 43 (2009) 2322–2327.
[37] P.H. Chang, Z.H. Li, T.L. Yu, et al., J. Hazard. Mater. 165 (2009) 148–155.
[38] J. Kang, H. Liu, Y.M. Zheng, J. Qu, J.P. Chen, J. Colloid Interface Sci. 354 (2010) 261–267.
[39] M.A. Gondal, X.F. Chang, Z.H. Yamani, Chem. Eng. J. 165 (2010) 250–257.
[40] M.B. Gawande, A. Goswami, F.X. Felpin, T. Asefa, X. Huang, et al., Chem. Rev. 116 (2016) 3722–3811.
[41] W.P. Xiong, Z.T. Zeng, X. Li, et al., Chemosphere 210 (2018) 1061–1069.
[42] G. Zhang, J. Qu, H. Liu, A.T. Cooper, R. Wu, Chemosphere 68 (2007) 1058–1066.
[43] H. Xiong, D. Zou, D. Zhou, et al., Chem. Eng. J. 316 (2017) 7–14.
[44] Y. Zhang, J. Zhou, X. Chen, L. Wang, W. Cai, Chem. Eng. J. 369 (2019) 745–757.
[45] X. Chang, G. Ji, K. Shen, et al., J. Alloys. Compd. 482 (2009) 240–245.
[46] D. Zhang, H. Niu, X. Zhang, Z. Meng, Y. Cai, J. Hazard. Mater. 192 (2011) 1088–1093.

[47] G.L. Liu, J.H. Zhou, W.N. Zhao, Z.M. Ao, T.C. An, Chin. Chem. Lett. 31 (2020) 1966–1969.
[48] L. Duan, L. Li, Z. Xu, W. Chen, Environ. Sci. Proc. Impacts 16 (2014) 1462–1468.
[49] K. Hu, X. Xiao, X. Cao, J. Nan, et al., J. Hazard. Mater. 192 (2011) 514–520.
[50] J. Xue, S. Ma, Y. Zhou, Z. Zhang, M. He, ACS Appl. Mater. Interfaces 7 (2015) 9630–9637.
[51] X. Shi, M. Fujitsuka, Z. Lou, P. Zhang, T. Majima, J. Mater. Chem. A 5 (2017) 9671–9681.
[52] M.A. Gondal, X.F. Chang, Z.H. Yamani, Chem. Eng. J. 165 (2010) 250–257.
[53] Y. Gao, Y. Li, L. Zhang, et al., J. Colloid Interface Sci. 368 (2012) 540–546.
[54] R.A. Figueroa, A. Allison Leonard, A.A. Mackay, Environ. Sci. Technol. 38 (2004) 476–483.
[55] P. Niu, L. Zhang, G. Liu, H.M. Cheng, Adv. Funct. Mater. 22 (2012) 4763–4770.
[56] Y. Wang, Y. Zheng, S. Lu, et al., ACS Appl. Mater. Interf.aces 7 (2015) 6093–6101.
[57] J. Zhang, M. Zhang, C. Yang, X. Wang, Adv. Mater. 26 (2014) 4121–4126.